What is a seismic reflector like?

Nathalie Favretto-Cristini, Paul Cristini, Eric de Bazelaire

GEOPHYSICS, VOL. 74, NO. 1 (JANUARY-FEBRUARY 2009); P. T13–T23, 11 FIGS.
10.1190/1.3033216

What is a seismic reflector like?

Nathalie Favretto-Cristini[1], Paul Cristini[1], and Eric de Bazelaire[2]

ABSTRACT

The spatial region that is in the vicinity of an interface and actually affects the interface response, and hence the reflected wavefield, is of particular interest for the characterization of reflectors from a seismic viewpoint. This region is represented by a volume of integration of medium properties above and below the interface whose maximum lateral extent corresponds to the lateral extent of the interface Fresnel zone, and whose maximum vertical extent is equal to a thickness we evaluate approximately for subcritical incidence angles for a plane interface as well as for curved interfaces of anticline and syncline type. The maximum vertical extent might be larger than the seismic wavelengths for subcritical incidence angles close to the critical angle and for a strong impedance contrast at the interface. Although the part of the reflector volume lying below the interface and affecting traveltime measurements actually is smaller than described in previous studies, the whole part of the reflector volume that affects the amplitude of the reflected wavefield is larger than estimates in previous studies, which considered only the spatial region below the interface. For a syncline (respectively, an anticline), it is larger (respectively, smaller) than described for a plane interface. In addition to providing more physical insights into the wave reflection process, this study might have significant implications for seismic interpretation using amplitude-variation-with-angle methodologies.

INTRODUCTION

The basis of many seismic studies is ray theory (Červený, 2001). Nevertheless, as measured seismic data have a finite low-frequency content, it is accepted that seismic wave propagation is not limited to an infinitely narrow line called ray but is extended to a finite volume of space around the raypath (i.e., the first Fresnel volume) (Kravtsov and Orlov, 1990), which contributes to the received wavefield for each frequency. The first Fresnel volume (FV) and its intersection with an interface, called the interface Fresnel zone (IFZ), have received wide attention in past decades. These concepts are being developed continually, and they have found so many applications in seismology and seismic exploration that it is impossible here to review all the books and articles that consider them in relation to seismic wave propagation (Schleicher et al., 1997; Spetzler and Snieder, 2004; Zhou et al., 2005). Nevertheless, we will mention the works compiled in Červený (2001).

Červený and his coauthors have suggested two methods that include FV parameter calculations into the ray-tracing procedure in complex 2D and 3D structures. The first method, called Fresnel volume ray tracing (Červený and Soares, 1992), combines the paraxial ray approximation with dynamic ray tracing and is applicable only to zero-order waves (direct, reflected, and transmitted waves), whereas the second method, more accurate than the first, is based on network ray tracing (Kvasnička and Červený, 1994). Unfortunately, the second method can be applied only to waves arriving at receivers in first arrivals.

Kvasnička and Červený (1994, 1996a, 1996b) have derived analytic expressions for FVs of seismic body waves and for IFZ for simple structures with plane interfaces, offering deeper insight into the properties of FV and IFZ. It is interesting to note that FV boundaries with corresponding FZ also can be estimated by using the method of isochron rays (Iversen, 2004).

Of particular interest are the size of the IFZ and size of the volume of the reflector involved in reflection time measurements (Hagedoorn, 1954) because each can be related to horizontal and vertical resolutions of seismic methods (Sheriff, 1980; Lindsey, 1989). Until now, only the IFZ and penetration depth of the FV below the interface have been considered thus in studies. If seismic amplitudes at receivers must be evaluated, the interface reflectivity must be determined. It is well known that except for mathematical convenience, interfaces are not infinitely thin. The underlying question then is: Considering an isolated interface, how thick are the spatial regions, above and below the interface, that actually might affect the inter-

Manuscript received by the Editor 5 March 2008; revised manuscript received 21 July 2008; published online 29 December 2008.
[1]Formerly Université de Pau, Laboratoire de Modélisation et Imagerie en Géosciences de Pau (MIGP), CNRS, Pau, France; presently Centre National de la Recherche Scientifique, Laboratoire de Mécanique et d'Acoustique, Marseille, France. E-mail: favretto@lma.cnrs-mrers.fr; cristini@lma.cnrs-mrs.fr
[2]Deceased June 28, 2007

face response and hence the reflected wavefield measured at the receivers? In other words, what is a reflector like from a seismic viewpoint? That question is the focus of this paper.

As noted above, as most seismic wave propagation studies have kinematic objectives, only the IFZ and penetration depth of the FV below the interface have received special attention in recent years. They have been evaluated approximately by analytic expressions for the case of a plane homogeneous interface (i.e., a plane interface with no lateral change in its physical properties) (Kvasnička and Červený, 1996a) or by using network ray tracing (Kvasnička and Červený, 1994). Unfortunately, to our knowledge, the spatial region above the plane interface in the incidence medium, which also affects the interface response, has never been identified. In addition, very few works are devoted to computations of the IFZ at a curved interface. Moreover, most of these works are mainly concerned with the case of normal wave incidence onto the interface (Lindsey, 1989; Iversen, 2006).

We mention that Hubral and his coworkers found the projected FZ of a zero-offset reflection onto the subsurface reflector using a standard 3D common-midpoint (CMP) traveltime analysis, without knowing the reflector overburden (Hubral et al., 1993; Schleicher et al., 1997). We refer also to the work of Kvasnička and Červený (1994). Using network ray tracing, they performed FV and IFZ parameter calculations for the wave transmission process in simple 2D structures, such as a low-velocity body with a slightly curved shape embedded in a higher-velocity medium (Kvasnička and Červený, 1994). Contrary to the work of Hubral and his coworkers (Hubral et al., 1993; Schleicher et al. 1997), knowledge of the velocity model is required for computations. Kvasnička and Červený (1994) have concluded that the FV penetrates inside the low-velocity body with a penetration distance equal to the penetration distance for head waves.

Gelchinsky (1985) derived symmetrized invariant formulas for the computation of the IFZ and FV for media of complex structure (e.g., an inhomogeneous medium with curvilinear interfaces), the restriction being that the medium is considered locally homogeneous in the vicinity of the FZ center. The formulas for the IFZ were obtained with the help of the Kirchhoff approximation and expressions for the Fresnel size for a particular case, and on the basis of the reciprocity relation. Lindsey (1989) studied changes in the IFZ size for normal wave incidence when the reflector is either a syncline or an anticline, as compared with the IFZ size for a plane reflector. Unfortunately, all these formulas do not provide insights on the size of the volume of the curved reflector involved in reflection time and amplitude measurements. We propose to address this issue.

We extend Lindsey's study to the case of oblique wave incidence onto a spherically shaped interface of anticline or syncline type. We derive analytic expressions for the size of the IFZ. In addition, we estimate analytically the maximum vertical extension of the volume that actually contributes to seismic amplitude. This estimation is valid in the symmetry plane between the source and receiver and for subcritical incidence angles. The derived formulas are obtained by using the curvature transmission and reflection laws of Hubral and Krey (1980). The case of a plane interface being viewed as a special case of a spherically shaped interface, we derive the expression for the vertical extent of the effective reflection volume, valid in the symmetry plane between the source and receiver and for subcritical incidence angles. In addition, we propose an approximate analytic expression for penetration depth of the FV below the plane interface, which provides more accurate results than the analytic expressions given in Kvasnička and Červený (1996a).

The paper is organized in three sections. The first section provides overviews of the FV and IFZ concepts. The maximum lateral extent of the (curved or plane) reflector volume (i.e., the size of the IFZ) is determined as a function of the incidence angle, and as a function of the interface curvature for the two types of curved interface. In the second section, the size of the spatial regions above and below a (curved or plane) homogeneous interface, which actually affect the interface response and hence the reflected wavefield, is evaluated as a function of the incidence angle for subcritical incidence angles. The third section presents some illustrative results for a given medium configuration and for the three types of interface (e.g., plane, anticline, and syncline).

The influence of the wave incidence onto the interface, and the influence of the interface curvature, on the size of the reflector volume are investigated more particularly. The influence of the impedance contrast at a plane interface on the penetration depth of the FV is studied also. To check accuracy, the results are compared with analytically exact results and approximate results obtained by Kvasnička and Červený (1996a) for a given medium configuration. We find that, although the part of the reflector volume lying below the interface and affecting the traveltime measurements actually is smaller than described in previous studies, the whole part of the reflector volume, which affects the amplitude of the reflected wavefield, is larger than previously estimated. We also find that for the syncline, the part of the reflector volume that actually affects the reflected wavefield is larger than that described for a plane interface, whereas for an anticline it is smaller.

For the remainder of this paper, we assume that the interface of interest is isolated from all others. We mean that the distance between this interface and another interface is much larger than $V/2B$, where V is the medium velocity and B is the frequency bandwidth of the source. In addition, we consider only the P-P reflection.

MAXIMUM LATERAL EXTENT OF A REFLECTOR

We consider two homogeneous isotropic elastic half-spaces in welded contact at a curved interface. The spherically shaped interface, which can be of anticline or syncline type, is tangent at the point $M\,(0,0,z_M)$ to the plane $z = z_M$, which represents the plane interface of interest in this study. The xy-plane includes the point source S $(-x_S,0,0)$ and receiver R $(x_S,0,0)$. The vertical z-axis is directed downward. A spherical wave with a constant amplitude is generated by the source in the upper half-space. The spherical wave can be decomposed into an infinite sum of plane waves (PW) synchronous with each other at the time origin.

We consider the harmonic PW with frequency f, which propagates in the upper half-space with the velocity V_{P1} from S to R, after being reflected by the interface at the point M in a specular direction θ with respect to the normal to the interface (Figure 1). Let the traveltime of the specular reflected wave be t_{SMR}, which is the sum of the wave traveltime t_{SM} from the source S to the point M and the wave traveltime t_{MR} from the point M to the receiver R.

The set of all possible rays SM_iR with constant traveltime t_{SMR} defines the isochrone for the source-receiver pair (S,R) relative to the specular reflection SMR. This isochrone describes an ellipsoid of revolution tangent to the interface at M, and whose rotational axis passes through S and R, defined by

$$\frac{x^2}{\left(\frac{z_M}{\cos\theta}\right)^2} + \frac{y^2+z^2}{z_M^2} - 1 = 0. \quad (1)$$

This equation is valid whatever the curvature of the interface. The frequency-dependent spatial region that actually affects the reflected wavefield is known to be the Fresnel volume (FV) corresponding to the pair (S,R) and associated with the wave reflection at M.

By definition, the FV is formed by virtual diffraction points F so that the waves passing through these points interfere constructively with the specular reflected wave. This condition is fulfilled when the path-length difference is less than one-half of the wavelength $\lambda_1 = V_{P1}/f$ corresponding to the dominant frequency f of the narrow-band source signal (Kravtsov and Orlov, 1990)

$$|l_{SF} + l_{FR} - (l_{SM} + l_{MR})| \le \frac{\lambda_1}{2}, \quad (2)$$

or

$$|t_{SF} + t_{FR} - (t_{SM} + t_{MR})| \le \frac{1}{2f}, \quad (3)$$

the quantity l_{XY} denoting the distance between the point X and point Y, and t_{XY} denoting the traveltime from X to Y.

As is well known, the main contribution to the wavefield comes from the first FV as the rapid oscillatory responses of the higher-order FVs and Fresnel zones cancel out and give minor contributions to the wavefield (Born and Wolf, 1999). In our work, we restrict ourselves to the first FV, which is referred to simply as FV. The FV is represented by only the part of the volume bounded by two ellipsoids of revolution with foci at S and R, which are tangent to fictitious planes parallel to the plane $z = z_M$ and located at a distance $\lambda_1/4$ below and above the plane $z = z_M$ (Figure 1), which is situated above the interface of interest (e.g., plane, anticline, or syncline) in the upper half-space. The two ellipsoids of revolution are defined by

$$\frac{x^2}{\left(\frac{z_M}{\cos\theta} \pm \frac{\lambda_1}{4}\right)^2} + \frac{y^2+z^2}{\left(\frac{z_M}{\cos\theta} \pm \frac{\lambda_1}{4}\right)^2 - z_M^2\tan^2\theta} - 1 = 0. \quad (4)$$

In fact, as seismic wavefields are transient and large band, it is generally necessary to decompose the source signal into narrow-band signals for which monochromatic FV can be constructed for the prevailing frequency of the signal spectrum (Knapp, 1991).

The IFZ is defined as the extent of intersection of the FV by the interface, which here is spherically shaped. Unlike the case of a plane interface (Kvasnička and Červený, 1996a), the IFZ is not represented by an ellipse centered at the reflection point M when the source S and receiver R are situated at the same distance from the interface. Depending on whether the interface is of anticline or syncline type, the IFZ alters in shape appropriately, and its size might not be determined in the same way for both types. Following Hubral and Krey (1980), the radius of the interface curvature R_{int} is positive if the in-

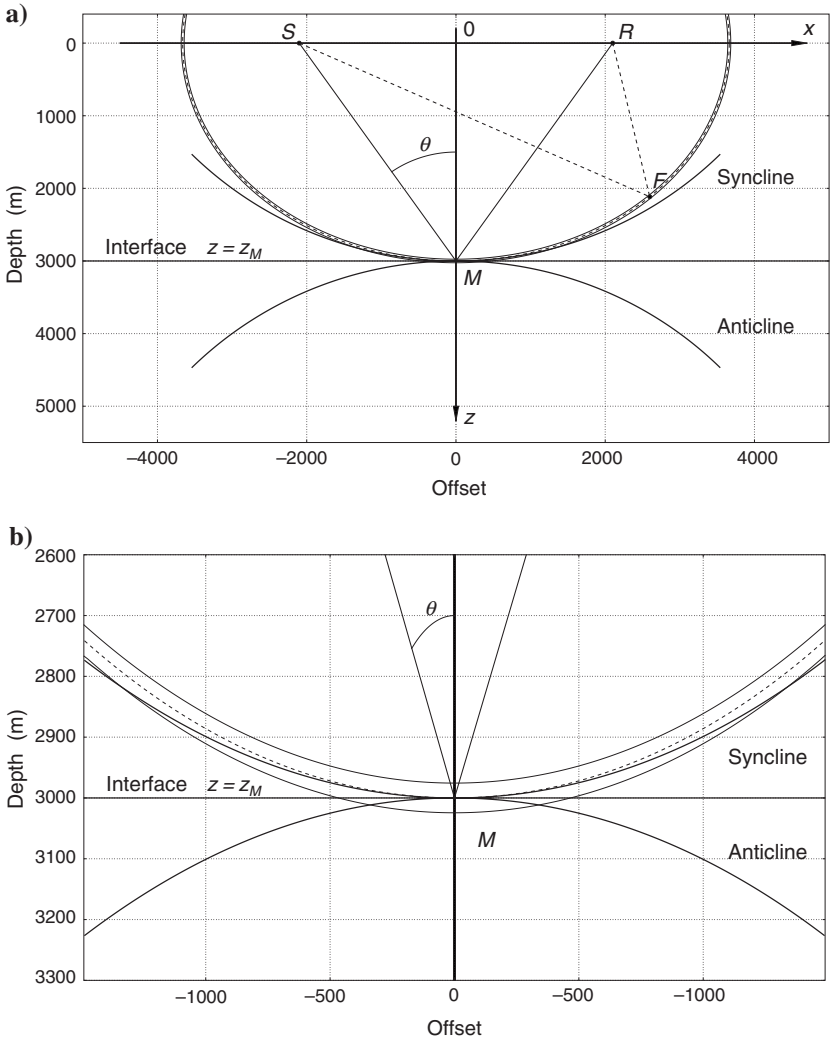

Figure 1. Representation, in the xz-plane, of the Fresnel volume involved in the wave reflection at the point M at a curved interface of anticline or syncline type under the incidence angle $\theta = 35°$. The source S and receiver R are situated at a distance $z_M = 3000$ m from the xy-plane tangent to the interface at the point M. The radius of the interface curvature is $R_{int} = \pm 5000$ m (positive for the anticline, negative for the syncline). Velocities of the upper and lower half-spaces are $V_{P1} = 2000$ m/s and $V_{P2} = 2800$ m/s, respectively, and the frequency $f = 25$ Hz. Seismic wavelengths in the upper and lower half-spaces then are $\lambda_1 = 80$ m and $\lambda_2 = 112$ m, respectively. The critical angle is equal to $\theta_C = 45.58°$. (a) The Fresnel volume is given by the volume between the ellipsoids of revolution with foci at S and R and located in the upper half-space (see the text for more details). (b) Focus on the Fresnel volume in the vicinity of the interfaces. The dashed line describes the isochron for the source-receiver pair (S,R) relative to the specular reflection SMR. The interface Fresnel zone, characterized by the extent of intersection of the Fresnel volume by the interfaces, is larger for the syncline than for the anticline.

terface appears convex to the incident wave. The radius R_{int} then is chosen positive for an anticline and negative for a syncline. This study extends the analysis by Lindsey (1989), who considered only the case of normal wave incidence onto the curved interface.

For Lindsey, the critical parameter that influences the size of the IFZ for a syncline is the ratio between the depth z_M of the reflection point M and radius of the interface curvature R_{int}. Note that the critical parameter actually is the ratio between the radius of curvature R_{iso} of the ellipsoid of revolution describing the isochrone for the pair (S,R) relative to the specular reflection SMR and radius of the interface curvature R_{int}, the radius R_{iso} being equal to the depth z_M for normal wave incidence. Depending on whether this ratio is less or larger than unity, the size of the IFZ is defined as the extent of intersection of the ellipsoid of revolution located at the distance $\lambda_1/4$ either above or below the plane $z = z_M$ by the syncline.

On the contrary, the size of the IFZ for an anticline is defined as the extent of intersection of the ellipsoid of revolution located at the distance $\lambda_1/4$ below the plane $z = z_M$ by the anticline, whatever the value of its radius of curvature R_{int}. For the sake of brevity, only the most relevant equations necessary for determining the size of the IFZ for an anticline are presented hereafter. Equations relative to the syncline can be derived easily from equations relative to the anticline by replacing the (positive) radius of the anticline curvature R_{int} by the (negative) radius of the syncline curvature R_{int}.

First we define the maximum lateral semiextent x_{max} of the IFZ following the x-axis in the xz-plane. In this plane, the anticline with the curvature center $C^+(0,z_M + R_{int})$ is represented by a circle defined by

$$x^2 + [z - (z_M + R_{int})]^2 = R_{int}^2. \tag{5}$$

Replacing the variable x by its expression obtained from the formulation of the ellipsoid of revolution, equation 4, and keeping only the sign + in the term $(z_M/\cos\theta \pm \lambda_1/4)^2$,

$$x^2 = a^2\left(1 - \frac{z^2}{b^2}\right), \tag{6}$$

where $a = z_M/\cos\theta + \lambda_1/4$ and $b = (a^2 - z_M^2\tan^2\theta)^{1/2}$, we obtain an equation of the second degree in the unknown z whose solutions z_1 and z_2 are

$$z_{1,2} = \frac{z_M + R_{int} \pm \Delta^{1/2}}{1 - \frac{a^2}{b^2}}, \tag{7}$$

where $\Delta = (z_M + R_{int})^2 - (1 - a^2/b^2)[a^2 + z_M(z_M + 2R_{int})]$ is always positive. Keeping only the solution z_1 or z_2 for which the inequality $1 - z^2/b^2 > 0$ is satisfied, and hence for which the variable x is positive, we deduce the maximum lateral semiextent x_{max} of the IFZ following the x-axis in the plane of incidence from equation 6 so that

$$x_{max} = a\left\{1 - \frac{z_{1,2}^2}{b^2}\right\}^{1/2}. \tag{8}$$

In the yz-plane, the ellipsoid of revolution located at the distance $\lambda_1/4$ below the plane $z = z_M$ is reduced to a circle defined by

$$y^2 + z^2 = b^2, \tag{9}$$

whereas the anticline is a circle defined by

$$y^2 + [z - (z_M + R_{int})]^2 = R_{int}^2. \tag{10}$$

The maximum lateral semiextent y_{max} of the IFZ following the y-axis in the yz-plane, i.e., in the direction perpendicular to the plane of incidence, then is given by the intersection of these two circles,

$$y_{max} = \left\{b^2 - \left[z_M + \frac{\lambda_1}{4}\left(\frac{z_M}{\cos\theta} + \frac{\lambda_1}{8}\right)(z_M + R_{int})^{-1}\right]^2\right\}^{1/2}, \tag{11}$$

where the quantity in the square root bracket is always positive.

The characteristics x_{max} and y_{max} of the IFZ at the surface of the anticline depend on the position of the source-receiver pair and on the incidence angle θ of the ray SM. The IFZ becomes larger in the incidence plane than in the transverse plane as the angle θ increases. Moreover, larger portions of the interface are involved for low-frequency than for high-frequency components of the wavefield. The characteristics x_{max} and y_{max} of the IFZ also depend on the radius of the interface curvature R_{int}. For the anticline, the IFZ becomes larger in the incidence plane than in the transverse plane as the radius of the interface curvature R_{int} increases. For sufficiently great radius R_{int}, the IFZ for the anticline is identical to the IFZ for the plane interface $z = z_M$. It is represented by an ellipse centered at the reflection point M whose in-plane semiaxis x_{max} and transverse semiaxis y_{max} are expressed as (Kvasnička and Červený, 1996a)

$$x_{max} = y_{max}\left[1 - \frac{z_M^2\tan^2\theta}{\left(\frac{z_M}{\cos\theta} + \frac{\lambda_1}{4}\right)^2}\right]^{-1/2}, \quad y_{max} = \left[\frac{\lambda_1}{2}\left(\frac{z_M}{\cos\theta} + \frac{\lambda_1}{8}\right)\right]^{1/2}. \tag{12}$$

Here, we must clarify some important points. Use is made in many papers of the classical representation of the FV, which is an ellipsoid of revolution with foci located at the receiver R and at the image source S″ situated symmetrically to the source S on the other side of the plane interface (Figure 2). This representation, mainly based on transmission considerations, is suitable to account for heterogeneities of the medium body located in the vicinity of the rays SM and MR, whereas the FV representation we use is more appropriate to account for heterogeneities of the interface, as it is connected strictly to the wave reflection process.

Moreover, unlike the classical one, this representation allows in a straightforward manner the definition of volumes above and below the interface, which characterize the reflector. The following section is focused on this definition. Note that the two FV representations are complementary and must be combined if wave propagation in media with heterogeneities in the medium body and at the interface is investigated.

MAXIMUM VERTICAL EXTENT OF A REFLECTOR

It is well known that the FV of the reflected wave is not limited by the interface, but penetrates across the interface in the lower half-space (Hagedoorn, 1954). The penetration depth can be evaluated approximately in an analytic way following traveltime measurements (Kvasnička and Červený, 1996a) or in a numerical way, using

network ray tracing (Kvasnička and Červený, 1994). We propose to derive analytically, in a straightforward manner, an approximate expression for the penetration depth of the FV across the curved interface, valid in the plane of symmetry between S and R and for subcritical incidence angles. This new expression provides more accurate results than those obtained by Kvasnička and Červený.

The curvature transmission law described in Hubral and Krey (1980, p. 43),

$$K_2 = K_1 \frac{V_{P2}}{V_{P1}} \left(\frac{\cos\theta}{\cos\theta'} \right)^2 + \frac{K_{int}}{\cos\theta'} \left(\frac{V_{P2}}{V_{P1}} \frac{\cos\theta}{\cos\theta'} - 1 \right), \quad (13)$$

connects the curvature K_2 of the transmitted wavefront to the curvature K_1 of the incident wavefront and to the interface curvature K_{int}. The transmission angle θ' is connected to the incidence angle θ through Snell's law, and V_{P2} denotes the velocity in the lower half-space. In the case of a curved interface, because the interface curvature K_{int} is different from zero, the curvature transmission law, equation 13, becomes in terms of radii of curvature R_2 and R_1 of the transmitted and incident wavefronts, respectively,

$$\frac{1}{R_2} = \frac{1}{R_1} \frac{V_{P2}}{V_{P1}} \left(\frac{\cos\theta}{\cos\theta'} \right)^2 + \frac{1}{R_{int}\cos\theta'} \left(\frac{V_{P2}}{V_{P1}} \frac{\cos\theta}{\cos\theta'} - 1 \right), \quad (14)$$

where R_{int} denotes the radius of the interface curvature.

By substituting the radii of curvature R_1 and R_2 for their respective expressions $z_M/\cos\theta$ and $z_{S'}/\cos\theta'$, we get the position $z_{S'}$ of the new fictitious source-receiver pair (S',R') with respect to the plane $z = z_M$, as a function of the incidence angle θ,

$$z_{S'} = \frac{z_M V_{P1} \cos^3\theta'}{V_{P2}\cos^3\theta + \frac{z_M}{R_{int}}(V_{P2}\cos\theta - V_{P1}\cos\theta')}. \quad (15)$$

The pair (S',R') can be viewed as an image of the pair (S,R) for the transmission process (Figure 3). That means that this fictitious source-receiver pair provides the same wavefront curvature as the pair (S,R). Unlike the real transmission process, which involves the upper and lower half-spaces, the wavefront relative to (S',R') propagates entirely in the lower half-space as if the upper half-space did not exist. This procedure is similar to the well-known procedure applied for the reflection process, which consists of replacing the pair (S,R) by its mirror image (S'',R'') (Figure 2).

As above, by considering the ellipsoid of revolution with foci S' and R' tangent to the plane $z = z_M$ at M (Figure 3),

$$\frac{x^2}{\left(\frac{z_{S'}}{\cos\theta'} \right)^2} + \frac{y^2 + z^2}{z_{S'}^2} - 1 = 0, \quad (16)$$

and the new ellipsoids that bound the FV associated with the reflection $S'MR'$,

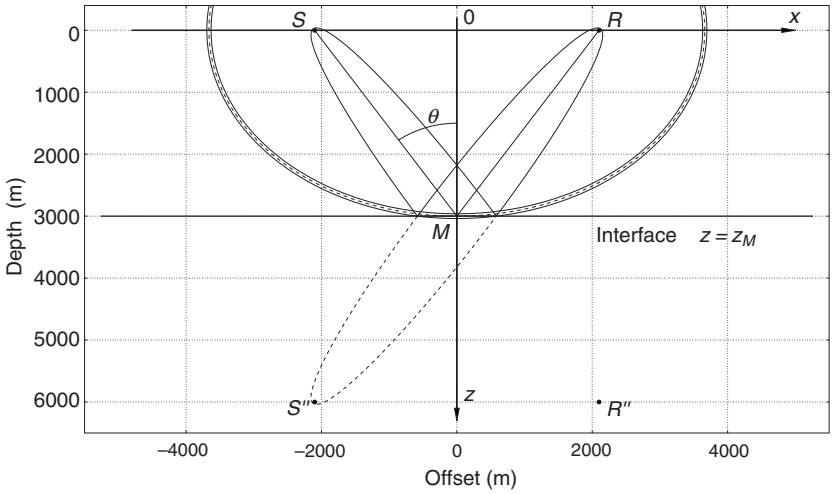

Figure 2. Representations, in the xz-plane, of the Fresnel volume involved in the wave reflection at the point M at the plane interface under the incidence angle $\theta = 35°$. The source S and receiver R are situated at a distance $z_M = 3000$ m from the interface. The classical representation of the Fresnel volume is based on the ellipsoid of revolution with foci located at R and at the mirror image S''. Another representation of the Fresnel volume associated with the reflection SMR is given by the volume located in the upper half-space between the ellipsoids of revolution with foci at S and R (see the text and Figure 1 for more details). See the legend of Figure 1 for medium properties.

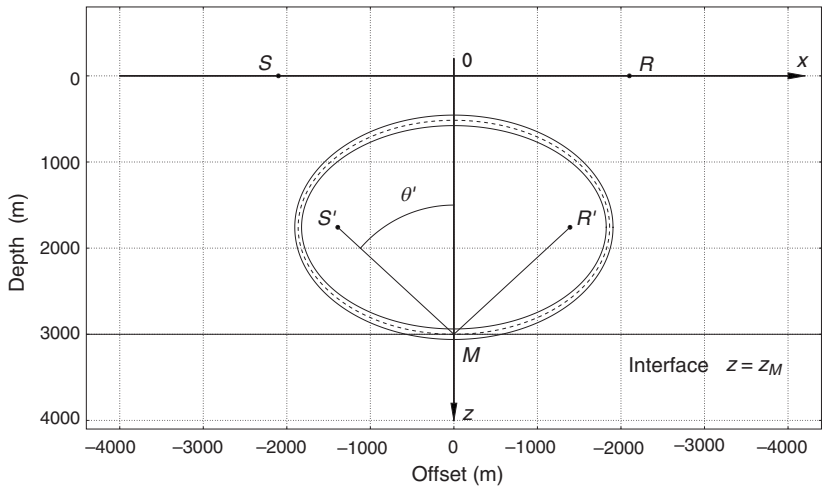

Figure 3. Representation, in the xz-plane, of the Fresnel volume involved in the fictitious wave reflection at the point M at a plane interface under the incidence angle θ'. The fictitious source-receiver pair (S',R') located at a distance $z_{S'}$ from the interface plane can be viewed as an image of the pair (S,R) for the transmission process. It provides the same wavefront curvature as (S,R) and propagates entirely in the lower half-space, as if the upper half-space did not exist. See the legend of Figure 1 for medium properties.

$$\frac{x^2}{\left(\frac{z_{S'}}{\cos\theta'} \pm \frac{\lambda_2}{4}\right)^2} + \frac{y^2 + z^2}{\left(\frac{z_{S'}}{\cos\theta'} \pm \frac{\lambda_2}{4}\right)^2 - z_{S'}^2 \tan^2\theta'} - 1 = 0, \tag{17}$$

it is straightforward to evaluate approximately the maximum penetration depth D_2, in the lower half-space, of the FV associated with the specular reflection *SMR*,

$$D_2 = \left[\left(\frac{z_{S'}}{\cos\theta'} \pm \frac{\lambda_2}{4}\right)^2 - z_{S'}^2 \tan^2\theta'\right]^{1/2} - z_{S'} = \left(z_{S'}^2 + \frac{\lambda_2 z_{S'}}{2\cos\theta'} + \frac{\lambda_2^2}{16}\right)^{1/2} - z_{S'}. \tag{18}$$

Because this expression is evaluated locally in the plane of symmetry between S and R and for subcritical incidence angles θ, it is valid whatever the radius of the interface curvature R_{int}. Nevertheless, the expression for the position $z_{S'}$ of the fictitious pair (S',R'), equation 15, differs following the radius of the interface curvature R_{int}. The penetration depth out of the plane of symmetry between S and R also can be evaluated in the same way from the envelope of the ellipsoids of revolution with foci S' and R' moving along caustics. Nevertheless, for postcritical incidence angles, we cannot define the penetration depth of the FV below the interface by using the curvature transmission law, because total reflection occurs.

Note that equation 18 provides only approximate evaluation of the actual penetration depth of the FV below the interface because the derivation based upon the curvature transmission law of Hubral and Krey (1980) does not take into account the fact that the incidence angle for the penetrating rays is not identical to the incidence angle of the central specular reflected ray. Expansion of equation 18 shows that for the values of the incidence angle θ close to zero, and then for great position $z_{S'}$, the first-order approximation to penetration depth D_2 with respect to $1/z_{S'}^2(\lambda_2 z_{S'}/2\cos\theta' + \lambda_2/8)$ corresponds to the approximation given by equation 38 in Kvasnička and Červený (1996a),

$$D_2 \simeq \frac{\lambda_2}{4\cos\theta'}. \tag{19}$$

Following the same reasoning, it seems clear that a region above the interface in the upper half-space also contributes to the interface response, and hence to the reflected wavefield. The maximum thickness D_1 of this region can be evaluated in the plane of symmetry between S and R and for subcritical incidence angles θ in the same way as above, the pair (S'',R'') being viewed as a mirror image of the pair (S,R) with respect to the plane $z = z_M$ (Figure 2),

$$D_1 = \left(z_{S''}^2 + \frac{\lambda_1 z_{S''}}{2\cos\theta} + \frac{\lambda_1^2}{16}\right)^{1/2} - z_{S''}. \tag{20}$$

We must determine the position $z_{S''}$ of the pair (S'',R''). The curvature reflection law in Hubral and Krey (1980, p. 43),

$$K_2 = K_1 + \frac{2K_{\text{int}}}{\cos\theta}, \tag{21}$$

becomes, in terms of radii of curvature R_2 and R_1,

$$\frac{1}{R_2} = \frac{1}{R_1} + \frac{2}{R_{\text{int}}\cos\theta}. \tag{22}$$

By substituting the radii of curvature R_1 and R_2 for their respective expressions $z_M/\cos\theta$ and $z_{S''}/\cos\theta$, we get the position $z_{S''}$ of the new fictitious source-receiver pair (S'',R'') with respect to the plane $z = z_M$, as a function of the incidence angle θ,

$$z_{S''} = \frac{z_M R_{\text{int}}\cos^2\theta}{2z_M + R_{\text{int}}\cos^2\theta}. \tag{23}$$

For the case of a plane interface, the radius of the interface curvature R_{int} tends to infinity, and the position $z_{S''}$ is equal to z_M. Unlike the penetration depth D_2, we can evaluate exactly the thickness D_1 for a plane interface, in the plane of symmetry between S and R, whatever the incidence angle θ, except for grazing angles. We also can evaluate exactly the distance D_1 out of the plane of symmetry in the same way as above because the caustics along which the foci S'' and R'' move are degenerate and then are reduced to points. Unlike the case of the plane interface, however, we no longer can evaluate exactly the thickness D_1 above a curved interface for subcritical incidence angles θ in the plane of symmetry between S and R, because the caustics along which the foci S'' and R'' move are no longer degenerate and thus are not reduced to points.

We can define now what a reflector is like from the seismic viewpoint. A reflector is a volume of integration of medium properties above and below the interface. This volume is represented by spatial regions with the maximum thicknesses D_1 and D_2 evaluated in the plane of symmetry between the source and receiver (Figure 4). Its maximum lateral extent corresponds to the lateral extent of the IFZ, and its maximum vertical extent corresponds to the thickness $D = D_1 + D_2$. In this work, we consider that the elastic media in contact are homogeneous and isotropic, which is an ideal case. The presence of heterogeneities or anisotropy in the media body might modify the size of the reflector volume, and more specifically the expres-

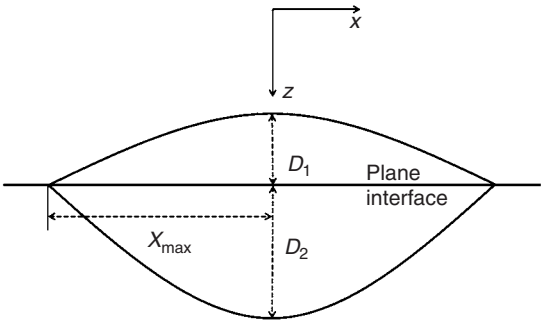

Figure 4. Schematic description of a seismic plane reflector in the xz-plane, i.e., the spatial region in the vicinity of the interface, which actually affects the interface response. The in-plane semiextent of the interface Fresnel zone is denoted by x_{max}. The distance D_1 is the maximum thickness of the region above the interface in the upper half-space, whereas the distance D_2 characterizes the penetration distance of the Fresnel volume (associated with the reflected wave *SMR*) below the interface in the lower half-space. These distances are evaluated in the plane of symmetry between the source and receiver and for subcritical incidence angles.

sions for the IFZ and thicknesses D_1 and D_2. It would be interesting to analyze the effect of anisotropy of the media on the size of the reflector volume. Our future contributions will focus on this topic.

RESULTS AND DISCUSSION

To illustrate the theoretical derivations, two cases of curved interfaces and one case of plane interface between elastic half-spaces are chosen. The source-receiver plane is located at a distance $z_M = 3000$ m from the plane tangent to the curved interfaces, which can be of anticline or syncline type. The radius of the interface curvature R_{int} is equal to ± 5000 m. It is positive for an anticline and negative for a syncline. The plane $z = z_M$ represents the plane interface of interest. The velocities of the upper and lower half-spaces are $V_{P1} = 2000$ m/s and $V_{P2} = 2800$ m/s, respectively. The frequency f being chosen is 25 Hz, and seismic wavelengths in the upper and lower half-spaces then are $\lambda_1 = 80$ m and $\lambda_2 = 112$ m, respectively. The critical angle is equal to $\theta_C = 45.58°$.

Figure 5 depicts the variation in size of the IFZ for an anticline and a syncline, as a function of the incidence angle θ, for the given value of the radius of the interface curvature R_{int}. The variation in size of the IFZ for a plane reflector also is shown for comparison. For $\theta = 0$ and for a given type of interface, the in-plane semiextent $x_{\max}$ and transverse semiextent $y_{\max}$ are equal. Following the type of interface, the IFZ then is represented by either a plane or a curved disk. With increasing θ, the IFZ becomes larger and larger in the incidence plane than in the transverse plane.

This feature is more pronounced for the syncline, the maximum size in the incidence plane being reached at a particular incidence angle θ, where the radius of the interface curvature R_{int} approaches the radius of curvature R_{iso} of the ellipsoid of revolution describing the isochrone for the source-receiver pair relative to the specular reflection *SMR*. This is shown more clearly in Figure 6, which depicts the variation in size of the IFZ for an anticline and a syncline, as a function of the radius of the interface curvature R_{int}, for a given incidence angle θ. When the radius R_{iso} is larger than the threshold value leading to the maximum size of the IFZ in the incidence plane, the in-plane semiextent $x_{\max}$ then decreases because the IFZ no longer is defined as the intersection of the ellipsoid of revolution located at the distance $\lambda_1/4$ below the plane $z = z_M$ by the syncline, but rather as the intersection of the ellipsoid located at the distance $\lambda_1/4$ above the plane $z = z_M$ by the syncline (Figure 1).

As suggested above, the critical parameter therefore is the ratio between the radius R_{iso} and radius R_{int}. We can show easily after straightforward calculations that for the syncline, the IFZ in the incidence plane is increased in size, as compared with that for a plane interface, approximately by the factor

$$F_S = \left(1 + \frac{z_M}{R_{\text{int}}} \frac{\beta^2}{\beta^2 - z_M^2 \tan^2 \theta}\right)^{-1}, \tag{24}$$

with negative radius R_{int} and $\beta = z_M/\cos\theta \pm \lambda_1/4$, the sign + (respectively, −) corresponding to the choice of the ellipsoid of revolution located at the distance $\lambda_1/4$ below (respectively, above) the plane $z = z_M$.

For the anticline, the IFZ in the incidence plane is decreased in size, as compared with that for a plane interface, approximately by the factor

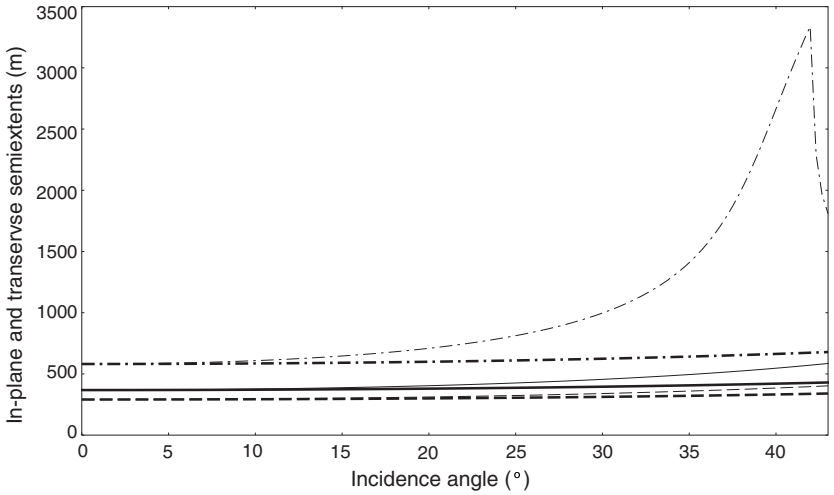

Figure 5. Variation in the size of the interface Fresnel zone at the surface of an anticline (dashed line) and a syncline (dash-dot line), as a function of the incidence angle θ, as compared with the results for a plane interface (solid line). Light curves are associated with the in-plane semiextent $x_{\max}$ (in the incidence plane); bold curves represent the variation in the transverse semiextent $y_{\max}$ (in the plane perpendicular to the incidence plane). See the legend of Figure 1 for medium properties.

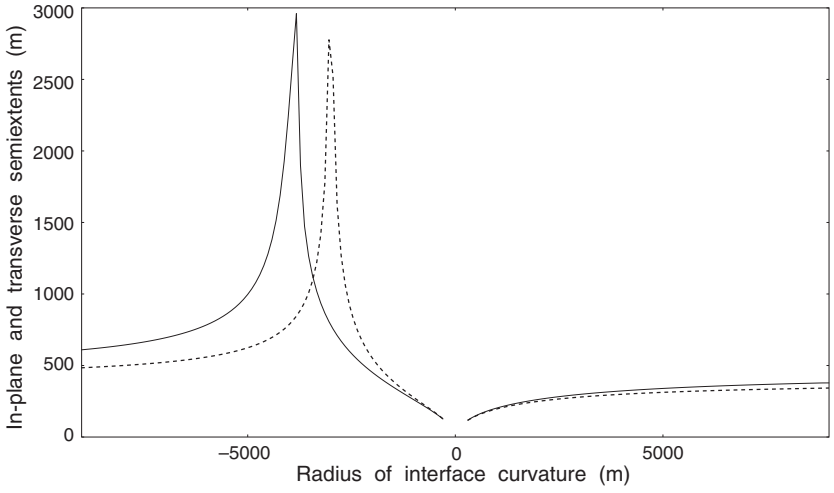

Figure 6. Variation in the in-plane semiextent $x_{\max}$ (solid lines) and in the transverse semiextent $y_{\max}$ (dashed lines) of the interface Fresnel zone at the surface of an anticline (positive radius of interface curvature) and a syncline (negative radius of interface curvature), as a function of the radius of interface curvature R_{int}. The incidence angle θ is equal to 30°. See the legend of Figure 1 for medium properties.

$$F_A = \left(1 + \frac{z_M}{R_{\text{int}}} \frac{a^2}{a^2 - z_M^2 \tan^2 \theta}\right)^{-1}, \qquad (25)$$

with positive radius R_{int} and $a = z_M/\cos\theta + \lambda_1/4$. The factors F_S and F_A tend to those given in Lindsey (1989) when the wave incidence is normal to the interface.

Similar conclusions can be drawn for the variation in the maximum semiextent $y_{\max}$ of the IFZ in the transverse plane for the anticline and syncline. The critical parameter that influences the length $y_{\max}$ is the ratio between the radius of curvature R_{iso} of the ellipsoid of revolution describing the isochrone for the source-receiver pair relative to the specular reflection *SMR* in the transverse plane (i.e., the depth z_M of the reflection point M) and radius of the interface curvature R_{int}. For the anticline (respectively, the syncline), the IFZ in the transverse plane is decreased (respectively, increased) in size, as compared with that for a plane interface, approximately by the factor

$$F = \left(1 + \frac{z_M}{R_{\text{int}}}\right)^{-1}, \qquad (26)$$

with positive radius R_{int} for the anticline and negative radius R_{int} for the syncline. Note in Figure 6 that when the value of the radius of the interface curvature R_{int} tends to infinity, the size of the IFZ for a curved interface tends to that for a plane interface.

Figure 7 shows the variation in penetration depth D_2 as a function of the incidence angle θ, for a given value of the radius of the interface curvature R_{int} for the anticline and syncline, whereas Figure 8 presents the variation in penetration depth D_2 as a function of the incidence angle θ for a plane interface. To check the accuracy of our approximation, the approximate results provided by equation 18 were compared with the exact values (Appendix A) for the anticline and syncline. For $\theta = 0°$, the penetration depth D_2 equals the well-known value $\lambda_2/4$ (Kvasnička and Červený, 1996a), as for the plane interface (Figure 8).

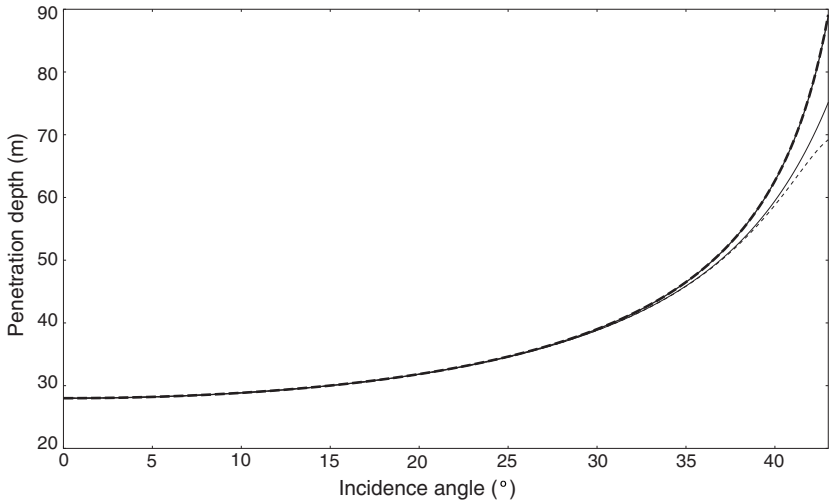

Figure 7. Variation in the penetration depth D_2 as a function of the incidence angle θ for an interface of anticline (light curves) or syncline (bold curves) type. Comparison of results provided by our approximation (dashed lines) with the exact solution (solid lines). See the legend of Figure 1 for medium properties.

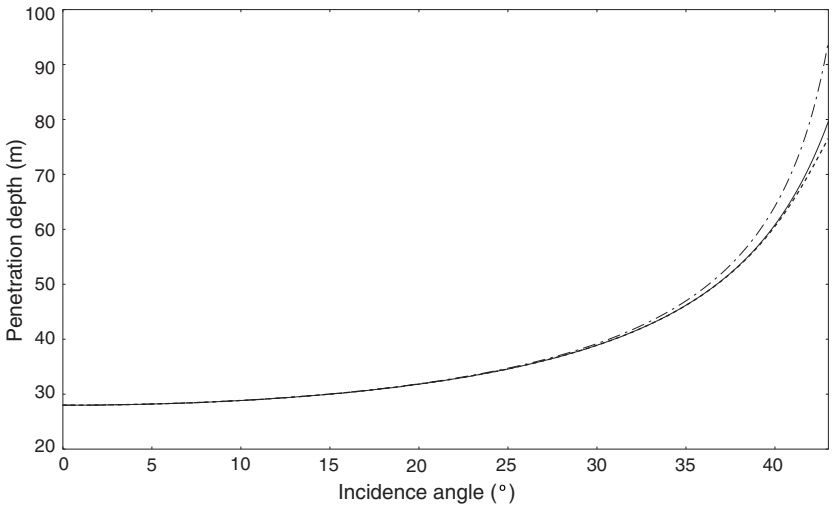

Figure 8. Variation in the penetration depth D_2 as a function of the incidence angle θ for a plane interface. Comparison of results provided by our approximation (dashed line) with exact solution (solid line) and results predicted by the approximation of Kvasnička and Červený (1996a) (dash-dot line).

Inspection of Figure 7 shows that the penetration depth D_2 increases with increasing subcritical angle θ, but it is always less than the seismic wavelength λ_2. For the syncline, it can be larger than the seismic wavelength λ_1 for subcritical incidence angles θ close to the critical angle $\theta_C = 45.58°$. Moreover, the values for the depth D_2 provided by our approximation deviate only slightly from the exact values for the syncline, the discrepancies being less than 0.01% up to the angle $\theta = 43°$, which is in the vicinity of the critical angle θ_C. For the anticline, however, the discrepancies do not exceed 0.01% up to the angle $\theta = 40°$ and 7.5% up to the angle $\theta = 43°$, our approximation underestimating the exact value for the penetration D_2.

Note that whatever the type of interface, the penetration depth D_2 has the same values for incidence angle θ lying between 0° and approximately 30°. For subcritical angles lying above 30°, the penetration depth D_2 for the syncline is, however, larger than that for the anticline. By comparing the curves obtained for the curved interfaces (Figure 7) and those obtained for the plane interface (Figure 8), we can note that the penetration depth D_2 for the syncline is increased in length, as compared with that for a plane interface, by approximately 16%, whereas the penetration depth D_2 for the anticline is decreased by approximately 10%.

Figure 8 shows the variations in the penetration depth D_2 as a function of the incidence angle θ provided by our approximation (equation 18), compared with the values obtained with the approximation of Kvasnička and Červený (1996a) (equation 19) and with the exact values (Appendix A). With increasing subcritical angle θ, the penetration depth D_2 increases, but it is always less than the seismic wavelength λ_2. Moreover, the values for D_2 provided by our approximation

deviate only slightly from the exact values. The discrepancies between them do not exceed 0.44% up to the angle $\theta = 40°$ and 4% up to the angle $\theta = 43°$, which is in the vicinity of the critical angle $\theta_C = 45.58°$.

On the contrary, the discrepancies between values for D_2 given by the approximation of Kvasnička and Červený (1996a) and the exact solution strongly increase with increasing angle θ, more particularly for angles above 30°. For $\theta = 43°$ the discrepancies exceed 23%. As a consequence, the part of a reflector below the interface, which actually affects the interface response and hence the reflected wavefield, is smaller than previous estimates. This conclusion has been found to come true whatever the medium configuration chosen. Nevertheless, for a given incidence angle θ the discrepancies between the values for D_2 provided by our approximation and those given by the approximation of Kvasnička and Červený (1996a) decrease with decreasing impedance contrast at the interface, as shown in Figure 9. For instance, for the impedance contrast equal to 1.2 and the incidence angle $\theta = 30°$, the discrepancy does not exceed 0.27%.

Figure 10 displays the variation in the thickness D_1 above the interface in the upper half-space, as a function of the incidence angle θ, for the given value of the radius of the interface curvature R_{int} for the anticline and syncline. To check the accuracy of our approximation, the approximate results provided by equation 20 were compared with the exact values (Appendix B). Approximate values for D_1 deviate only slightly from the exact values, the discrepancies between them lying below 0.05% up to the angle $\theta = 43°$.

Figure 10 also depicts the variation in the distance D_1, as a function of the incidence angle θ, for a plane interface. In this case, as mentioned above, the distance D_1 provided by equation 20 is evaluated exactly. Whatever the type of interface and for the normal wave incidence ($\theta = 0°$), the distance D_1 equals the value $\lambda_1/4$. The thickness D_1 increases with increasing incidence angles θ, but it is always less than the seismic wavelength λ_1 and penetration depth D_2. Moreover, the thickness D_1 is not much influenced by the interface curvature, the dicrepancies between the curves associated with the syncline and anticline being less than 1%.

In this work, we have identified the zone in the vicinity of a (plane or curved) interface that actually affects the interface reflectivity, and we have established the spatial limits of this effective reflector volume, which merits further investigation. Although these spatial limits might vary following the properties of the bulk media in contact resulting, for instance, from anisotropy or from the presence of heterogeneities, defining these limits for an ideal case (e.g., homogeneous and isotropic media in contact) enables us to fix ideas and provide a road map for future applications to real media.

In addition to providing more physical insights into the wave reflection process, our study could have significant implications for seismic interpretation using amplitude-variation-with-angle (AVA) methodologies. On the one hand, when amplitude measurements are considered, we must evaluate the interface reflectivity by considering the effective reflector volume that actually affects it, and by accounting for heterogeneities located within this volume. More specifically, we must select heterogeneities whose characteristic length, along with their spatial distribution within the reflector volume, might interact with properties of the incident wave, so as to derive a model of the effective behavior of the reflector volume.

A structural description of multiscaled heterogeneities located within the reflector volume must be considered, therefore, as a preliminary step toward the modeling of the interface response. Our future contributions will focus on this topic. However, we specify that in the absence of heterogeneity located within the reflector volume,

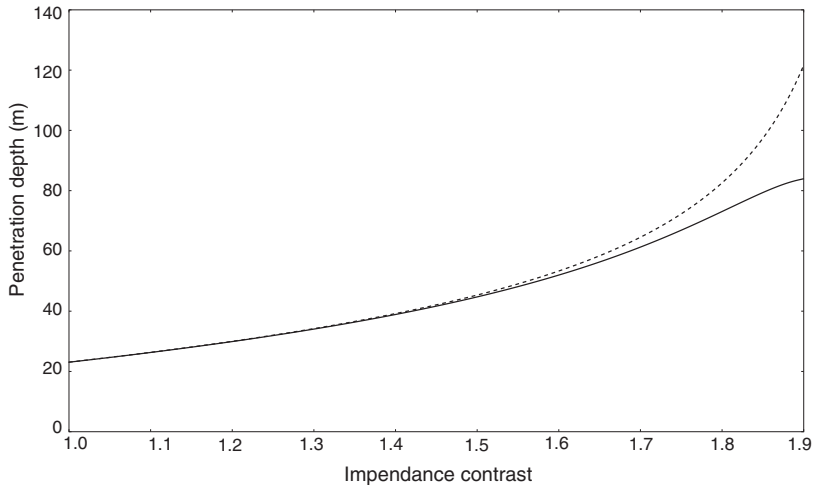

Figure 9. Variation in the penetration depth D_2 as a function of the impedance contrast at a plane interface for the incidence angle $\theta = 30°$. Comparison of results provided by our approximation (solid line) with results predicted by the approximation of Kvasnička and Červený (1996a) (dashed line).

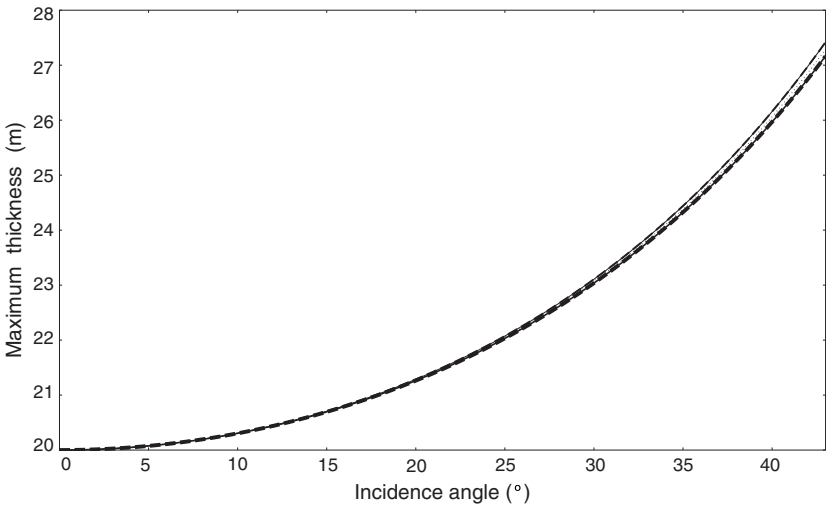

Figure 10. Variation in the maximum thickness D_1 as a function of the incidence angle θ for an interface of anticline (light curves) or syncline (bold curves) type and for a plane interface (dotted line). Comparison of results provided by our approximation (dashed line) with the exact solution (solid line). See the legend of Figure 1 for medium properties.

we must account for only the IFZ for modeling the interface response. In a previous work (Favretto-Cristini et al., 2007), we pointed out the consequences of ignoring the IFZ in forward modeling of seismic wave reflection. More specifically, for wide-angle AVA methodologies and near the critical incidence angle, the geometric spreading compensation no longer is sufficient to reduce the point-source amplitudes to plane-wave (PW) amplitudes predicted by Zoeppritz equations. The additional application of the IFZ concept to the PW theory is necessary to obtain the reflected P-wave amplitudes measured at receivers.

These results have significant implications for seismic interpretation using amplitudes: Assuming that the AVA curves corresponding to real measured data might be described well by the PW theory leads to biased estimations of the media properties, even in the ideal case of homogeneous isotropic media. Our present work is focused precisely on this particular aspect and will be reported later. On the other hand, when only traveltime measurements are considered, for instance for locating reflectors in the media, there is no need to define the region above the interface with the thickness D_1, because this region is already included in the classical representation of the FV, which is the ellipsoid of revolution with foci located at the receiver R and at the image source S'' (Figure 2). In this case, only the region below the interface with the thickness D_2 must be considered.

CONCLUSION

We have identified the zone in the vicinity of an interface that actually affects the interface reflectivity and hence the reflected wavefield. Our work extends previous studies to the case of the oblique wave incidence onto a plane interface, or onto a curved interface of anticline or syncline type, between two homogeneous and isotropic media. We have derived analytic expressions for evaluating approximately the spatial limits of the effective reflector volume.

A comparison with exact results has shown that our expressions provide more accurate results than those given in previous works. The effective reflector volume has its maximum lateral extent equal to the lateral extent of the interface Fresnel zone, and its maximum vertical extent equal to a thickness that might be larger than the seismic wavelength of the incident wave for great incidence angles close to the critical angle. Although the part of the reflector volume lying below the interface and affecting traveltime measurements actually is smaller than described in previous studies, the whole part of the reflector volume affecting the amplitude of the reflected wavefield is larger than previous estimates.

ACKNOWLEDGMENTS

The work reported here is the result of a fruitful collaboration during many years between us, Nathalie Favretto-Cristini and Paul Cristini, and our late friend Dr. Eric de Bazelaire. We consider ourselves extremely fortunate to have had the opportunity to work closely with a scientist of Dr. de Bazelaire's caliber.

We gratefully appreciate the careful reviews by J. P. Lindsey, B. Bednar, A. Stovas, and associate editor D. Draganov. We thank them for their valuable comments and suggestions to improve the manuscript. We also thank Jacques Blanco for his encouragement and enthusiasm for this work.

The work was supported in part by the Agence Nationale de la Recherche (ANR) under the EMSAPCO2 project.

APPENDIX A

EXACT DERIVATION OF THE PENETRATION DEPTH D_2 OF THE FRESNEL VOLUME FOR SUBCRITICAL INCIDENCE ANGLES

We consider the case of a spherically shaped interface of anticline type with the center of curvature C and radius of curvature R_{int}. As the source S and receiver R are located at the same distance from the plane tangent to the curved interface, the penetration zone of the FV is symmetrical, and its deepest point M' is located in the plane of symmetry between S and R (Figure A-1). The penetration distance D_2, which corresponds to the maximum distance D of the point M' from the reflection point M, can be determined mathematically by solving the optimization problem

$$D_2 = \max_{\alpha}\{D\}, \tag{A-1}$$

where

$$D = \left[\left(\frac{\lambda_1}{4} - l_{SA} + l_{SM}\right)^2\left(\frac{V_{P2}}{V_{P1}}\right)^2 - R_{\text{int}}^2\cos^2\alpha\right]^{1/2} + R_{\text{int}}(1 - \sin\alpha), \tag{A-2}$$

obtained from the definition of the Fresnel zone:

$$\frac{l_{SA}}{V_{P1}} + \frac{l_{AM'}}{V_{P2}} - \frac{l_{SM}}{V_{P1}} = \frac{1}{4f}, \tag{A-3}$$

where $l_{SA} = [(z_M \tan\theta + R_{\text{int}}\cos\alpha)^2 + (z_M + R_{\text{int}}(1 - \sin\alpha))^2]^{1/2}$, $l_{SM} = z_M/\cos\theta$, and $l_{AM'} = [R_{\text{int}}^2\cos^2\alpha + (D - R_{\text{int}}(1 - \sin\alpha))^2]^{1/2}$.

In the case of a plane interface, the penetration distance D_2 corresponds to the maximum distance D of M' from the interface plane $z = z_M$. As above, it can be determined mathematically by solving the optimization problem

$$D_2 = \max_{X}\{D\}, \tag{A-4}$$

where $X = l_{AM}$ and $D = [(\lambda_1/4 - l_{SA} + l_{SM})^2(V_{P2}/V_{P1})^2 - X^2]^{1/2}$,

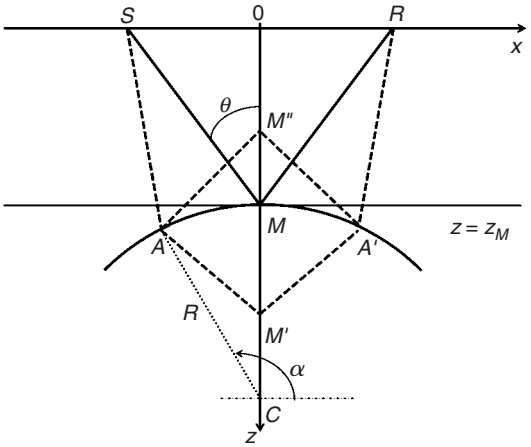

Figure A-1. Schematic description of the configuration for deriving the penetration depth D_2 of the Fresnel volume in the lower half-space and the thickness D_1 in the upper half-space for the case of a spherically shaped interface of anticline type with the center of curvature C and radius of curvature R_{int}.

obtained from the definition of the Fresnel zone with $l_{SA} = [(z_M \tan\theta - X)^2 + z_M^2]^{1/2}$ and $l_{AM'} = (X^2 + D^2)^{1/2}$.

APPENDIX B

EXACT DERIVATION OF THE MAXIMUM THICKNESS D_1 FOR SUBCRITICAL INCIDENCE ANGLES

Considering the configuration depicted in Figure A-1, the maximum thickness D_1, which corresponds to the maximum distance D' of the point M'' from the reflection point M, can be determined mathematically by solving the optimization problem

$$D_1 = \max_{\alpha}\{D'\}, \tag{B-1}$$

where

$$D' = \left[\left(\frac{\lambda_1}{4} - l_{SA} + l_{SM}\right)^2 - R_{\text{int}}^2\cos^2\alpha\right]^{1/2} - R_{\text{int}}(1 - \sin\alpha), \tag{B-2}$$

obtained from the definition of the FZ with $l_{AM''} = [R_{\text{int}}^2\cos^2\alpha + (D + R_{\text{int}}(1 - \sin\alpha))^2]^{1/2}$, the distances l_{SM} and l_{SA} being given in Appendix A.

REFERENCES

Born, M., and E. Wolf, 1999, Principles of optics, 7th exp. ed.: Cambridge University Press.

Červený, V., 2001, Seismic ray theory: Cambridge University Press.

Červený, V., and J. Soares, 1992, Fresnel volume ray tracing: Geophysics, **57**, 902–915.

Favretto-Cristini, N., P. Cristini, and E. de Bazelaire, 2007, Influence on the Interface Fresnel zone on the reflected P-wave amplitude modeling: Geophysical Journal International, **171**, 841–846.

Gelchinsky, B., 1985, The formulae for the calculation of the Fresnel zones or volumes: Journal of Geophysics, **57**, 33–41.

Hagedoorn, J. G., 1954, A process of seismic reflection interpretation: Geophysical Prospecting, **2**, 85–127.

Hubral, P., and T. Krey, 1980, Internal velocities from seismic reflection time measurements: SEG.

Hubral, P., J. Schleicher, M. Tygel, and C. Hanitzch, 1993, Determination of Fresnel zones from traveltime measurements: Geophysics, **58**, 703–712.

Iversen, E., 2004, The isochron ray in seismic modeling and imaging: Geophysics, **69**, 1053–1070.

———, 2006, Amplitude, Fresnel zone, and NMO velocity for PP and SS normal-incidence reflections: Geophysics, **71**, no. 2, W1–W14.

Knapp, R., 1991, Fresnel zones in the light of broadband data: Geophysics, **56**, 354–359.

Kravtsov, Y., and Y. Orlov, 1990, Geometrical optics of inhomogeneous media: Springer-Verlag, Springer Series on Wave Phenomena.

Kvasnička, M., and V. Červený, 1994, Fresnel volumes and Fresnel zones in complex laterally varying structures: Journal of Seismic Exploration, **3**, 215–230.

———, 1996a, Analytical expressions for Fresnel volumes and interface Fresnel zones of seismic body waves: Part 1 — Direct and unconverted reflected waves: Studia Geophysica et Geodetica, **40**, 136–155.

———, 1996b, Analytical expressions for Fresnel volumes and interface Fresnel zones of seismic body waves: Part 2 — Transmitted and converted waves. Head waves: Studia Geophysica et Geodetica, **40**, 381–397.

Lindsey, J., 1989, The Fresnel zone and its interpretative significance: The Leading Edge, **8**, 33–39.

Schleicher, J., P. Hubral, M. Tygel, and M. Jaya, 1997, Minimum apertures and Fresnel zones in migration and demigration: Geophysics, **62**, 183–194.

Sheriff, R., 1980, Nomogram for Fresnel-zone calculation: Geophysics, **45**, 968–972.

Spetzler, J., and R. Snieder, 2004, The Fresnel volume and transmitted waves: A tutorial: Geophysical Journal International, **69**, 653–663.

Zhou, Y., F. Dahlen, G. Nolet, and G. Laske, 2005, Finite-frequency effects in global surface-wave tomography: Geophysical Journal International, **163**, 1087–1111.